CERN-ACC-2020-0002
13-01-2020
androula.alekou@cern.ch

Report

Deliverable 2.10: Summary of the observations in the SPS and update of the estimates for HL-LHC

A. Alekou[1, 2], F. Antoniou[1], R. B. Appleby[2], H. Bartosik[1], R. Calaga[1], M. Carla[1], L. Carver[*1, 3], Y. Papaphilippou[1], C. Welsch[3]*
[1]CERN, Switzerland, [2]University of Manchester and Cockcroft Institute, [3]University of Liverpool

Abstract

Over the course of 2018, 7 machine developments were conducted for dedicated crab cavity measurements with each measurement slot consisting of 10 hours of SPS machine time [1]. During this period, many different sets of measurements and studies were performed to improve the understanding of the interaction between protons and crab cavities. This note describes the main results relating to beam dynamics. Additionally, the considerations on crab cavity related instrumentation required for HL-LHC are presented.

Keywords: Crab Cavities, HL-LHC, SPS tests, instrumentation.

[*]Now at ESRF, Grenoble, France.

Contents

1 Instrumentation observations during the SPS CC experiments

The world's first injection of a proton beam into a CC occurred on the 23^{rd} of May 2018 at 12:55. Shortly afterwards, the synchronisation between the SPS and the CC RF signal was setup and optimised and regular synchronous crabbing was observed. Figure 1 shows a reconstruction of the crabbing motion taken from the head-tail (HT) monitor. The optics parameters at the location of the cavities are shown in Table 1.

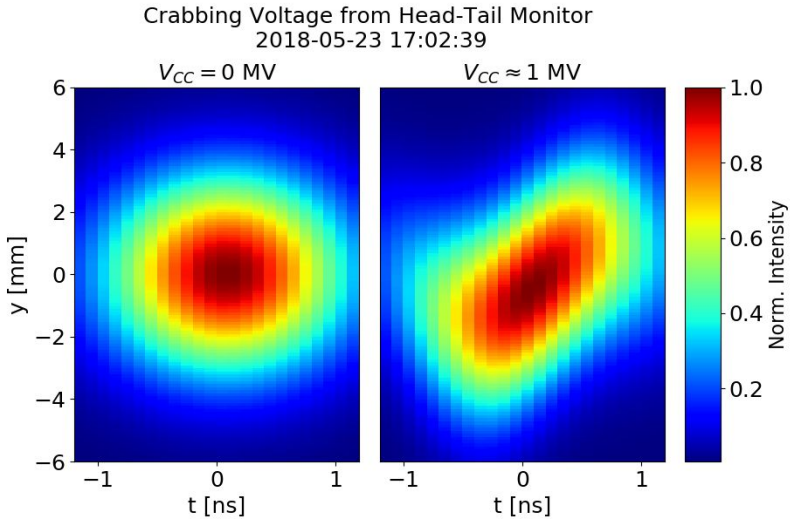

Fig. 1: Vertical off-set with respect to the longitudinal position of the particles when the CCs were OFF (left) and ON (right); the beam-shapes were simulated using the measured HT data.

Table 1: SPS CC parameter table

Parameter	Value
number of cavities	2
s-location [m]	6312.7213, 6313.3213
Plane of crabbing	Vertical
f [MHz]	400.528
β_{x1}, β_{y1} [m]	29.24, 76.07
β_{x2}, β_{y2} [m]	30.31, 73.82

1.1 Emittance growth in the SPS

During the SPS tests of May-November 2018, emittance growth measurements took place during two MDs. What needed to be studied was the level at which the cavity voltage feedback provides transverse kicks to the beam at frequencies which are resonant with the beam transverse motion as this could lead to unacceptably large emittance growth over time. The two MDs were performed in coast for time scales found in the operation of the LHC. An additional signal generator (range DC to 10 kHz) was mixed with the spectrum coming from the cavity feedback in order to control the amplitude of the feedback at the first betatron sideband i.e. control the strength at which the feedback is kicking at a specific resonant frequency (see Figure 2 [2]). The results from these measurements can be found in Fig. 3. As can be seen, the measured emittance growth is consistently a factor of 2 below the predictions [3]. This is a step in the positive direction, however more work needs to be performed in the future to understand the discrepancy.

1.2 RF Multipolar Components (a_3)

The non-linearity of the 400 MHz fundamental mode of the CC can give rise to higher order multipole components that can affect the beam dynamics in the machine (for example by reducing the dynamic

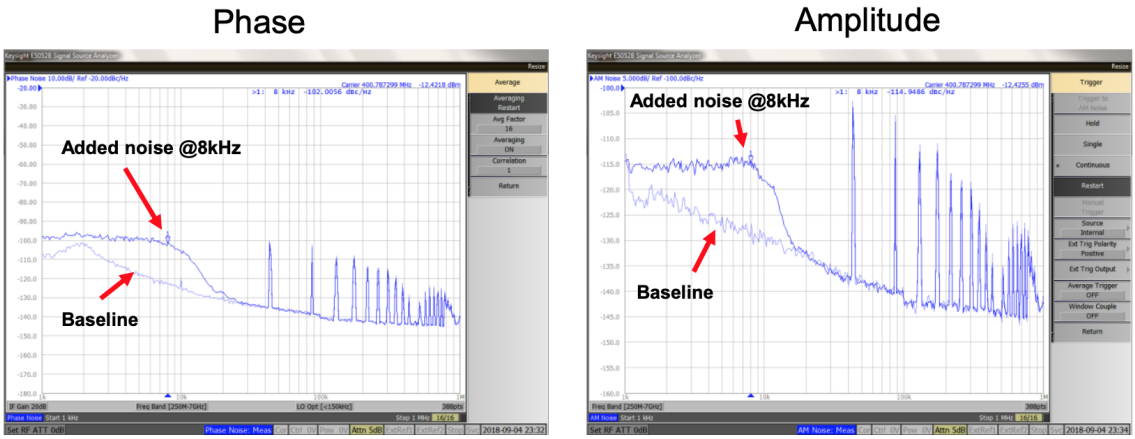

Fig. 2: Power density squared of the noise signal sent to the cavity feedback; the RF noise (phase and amplitude) covered a band from DC to 10 kHz and excited only the first betatron band (∼8 kHz).

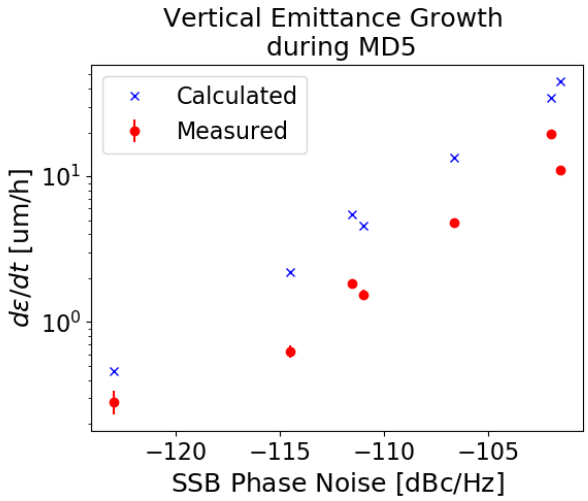

Fig. 3: Summary of emittance growth measurements as a function of the feedback noise at the frequency of the first betatron sideband.

aperture). These are of particular concern (as compared with static multipolar components) as they cannot be corrected due to the dependence on cavity parameters. Of primary concern with this particular CC model (DQW) is the skew sextupolar (a_3) component.

During the SPS CC tests, the a_3 was measured by kicking in the horizontal plane and measuring the vertical betatron motion driven by the skew sextupolar field. The vertical motion was thus decomposed in two main contributors: the spectral line V20, whose frequency is 2 times the horizontal tune, and the spectral line V00 (a change of the closed orbit), whose frequency is 0 [4]. The amplitude of V20 and V00 depend linearly on a_3, the horizontal action and a term depending on the optics. Therefore by comparing the turn-by-turn observation of the V20 and V00 spectral lines obtained from the BPMs, and an analytical model obtained from the first order perturbation theory it was possible to derive the value of a_3.

It can be seen that while the trends of the measured spectral lines V00 and V20 follow correctly the analytical model, a strong disagreement in terms of overall phase of the V20 spectral line is present. Such disagreement can be ascribed to the presence of non-linearities in the SPS optics that, along with the large vertical orbit produced by the CC, can affect by a feed-down effect the V00 and V20 spectral lines. A deep understanding of the SPS non-linear model is therefore necessary and an effort to work out the required details is being carried out.

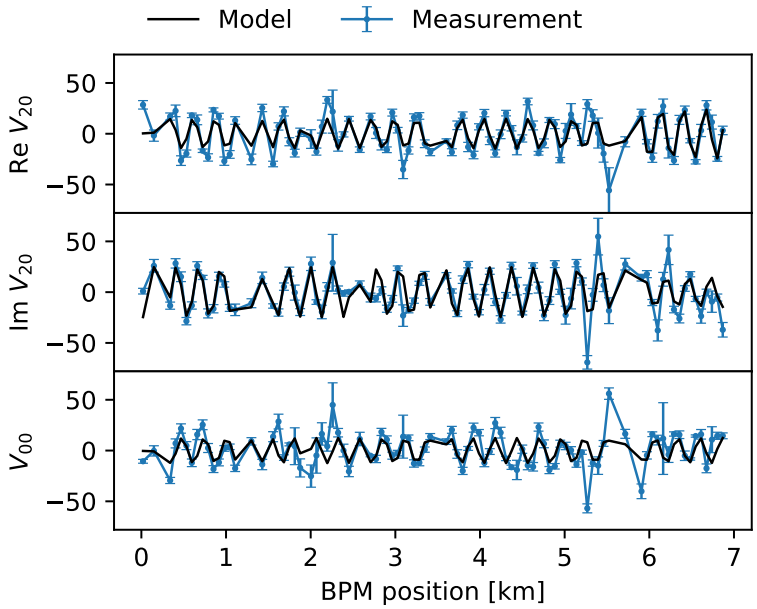

Fig. 4: Variation (blue) of the real and imaginary part of the V20 spectral line and the V00 closed orbit distortion induced by changing the CC voltage from ∼0 MV to ∼+1 MV. The analytical model (black) has been scaled in order to fit the measured data and determine a_3. Furthermore, to match the experimental data to the model, the measured V20 has been multiplied by a phase factor $e^{i\phi}$ with the phase ϕ equal to ∼40°, suggesting that the measurement is probably spoiled by some other sources of a_3 not present in the model.

1.3 Crab dispersion

As explained in [5] the effect of the CC on on a particle is like the one of an orbit corrector, or dipole, with the only difference being that the crab kick is z-dependent. Following the closed-orbit distortion approach, one can get the deviation of the crab closed orbit with a specific longitudinal position along the bunch:

$$x_{D_{CC}}(z,s) = \sqrt{\beta(s_0)\beta(s)}\frac{\theta}{2\sin\pi Q}\cos\big(\psi(s,s_0) - \pi Q\big) \tag{1}$$

where $\beta(s)$ and $\beta(s_0)$ are the beta functions along s and at the CC-location respectively, $\psi(s,s_0)$ is the phase advance between the CC and the s-location in the ring, and Q is the tune. The CC kick, θ, is given by:

$$\theta = \frac{V}{E}\sin(\kappa z + \phi) \tag{2}$$

where V, κ, ϕ are the CC voltage, wavenumber and phase respectively, E the particle energy and z the longitudinal position of the particle in the bunch (with respect to the bunch centre). A particle which only has $z = 1\sigma_z$ as initial offset will later be at $\delta_P = 1\sigma_P$ and $z = 0$ due to synchrotron oscillation. In order to arrive at a definition with the same units as the off-momentum dispersion for linear crab kicks within $\pm 1\sigma_z$, the "crab dispersion" is defined as the orbit deviation at $z = 1\sigma_z$ normalised to $1\sigma_P$ [5]:

$$D_{CC}(s) = \frac{x_{D_{CC}}(1\sigma_z, s)}{1\sigma_P}. \tag{3}$$

Some fundamental checks were made to compare the orbit response of the beam with simulations. This was of particular interest as it was not clear how the BPMs would respond to a crabbed bunch. Figure 5 shows the measured CC orbit distortion compared with the MAD-X calculation.

It was found that while the phase behaviour was in good agreement with the model for the SPS produced by MAD-X, the equivalent voltage needed to reproduce the behaviour was approximately a factor of 2 lower than what the other CC diagnostics were showing; i.e. the power sensors were measuring 1 MV, the HT monitor 1.2 MV (this value was provided using data coming from the calibration of the instrument), but the BPM response was showing 0.7 MV.

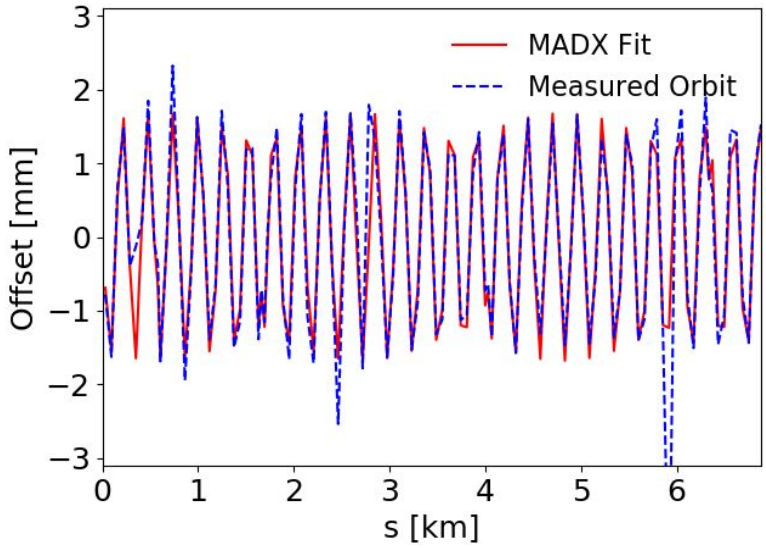

Fig. 5: Comparison of CC closed orbit with MAD-X fit.

Upon closer inspection, it was found that this difference has to be attributed to the characteristic spectral response of the BPM. The effective beam position measured by a BPM, whose spectral response follows the distribution $R(\omega)$ is obtained as:

$$\bar{X}^2 = \frac{\int |R(\omega) \cdot \mathcal{F}\{I(t) \cdot X(t)\}|^2 d\omega}{\int |R(\omega) \cdot \mathcal{F}\{I(t)\}|^2 d\omega} \tag{4}$$

where $I(t)$ is the bunch longitudinal distribution, $X(t)$ is the transverse position of the bunch slice with a delay t with respect to the bunch centre and $\mathcal{F}$ represents the Fourier transform operator. In the case of the Multi Orbit POsition System (MOPOS) BPMs installed in the SPS, $R(\omega)$ reduces to a δ distribution centred around 200 MHz. Figure 6 shows the measured beam position by a MOPOS BPM normalised by the actual peak orbit (or the orbit produced by a static field whose strength is equal to the peak CC field) as a function of the bunch-length, assuming a Gaussian longitudinal distribution.

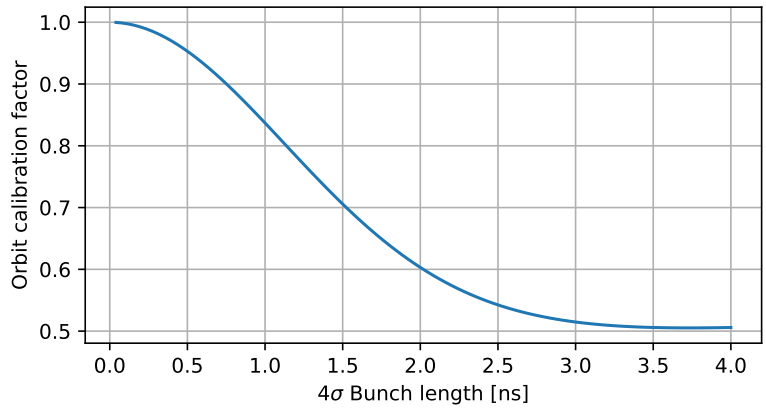

Fig. 6: Response of a MOPOS BPM obtained from Eq. (4) as a function of the bunch-length in the case of a longitudinal bunch distribution and assuming the beam on crest with respect to the CC field

Applying the proper correction to the CC closed orbit measurement shown in Fig. 5, where a 4σ bunch-length of 2.9 ns was observed, increases the estimated CC voltage to 1.34 MV, a value considered within the uncertainty of the RF measurement. The BPMs used in the LHC instead employ a wide bandwidth electronic.

1.4 Cavity transparency

A constant question for the surrounding operation of the CCs in the LHC was whether or not they can be transparent in the event of issues with the cavities, i.e. they can be counter phased such that the total crabbing on the beam is zero. The transparency is also being tested to understand how well the the orbit bump created by the cavity can be closed. During the last MD, with 1 MV in each cavity, the phases were optimised such that a total crabbing voltage of 60 kV was observed. Note that the 60 kV value was not obtained from a careful fitting of the full sinusoidal response but instead was taken from the online measurements during the MD as the best compensation. It can be seen clearly in Figure 7 that the beam response was minimal in transparent mode in both simulations (top) and measurement (bottom, green line).

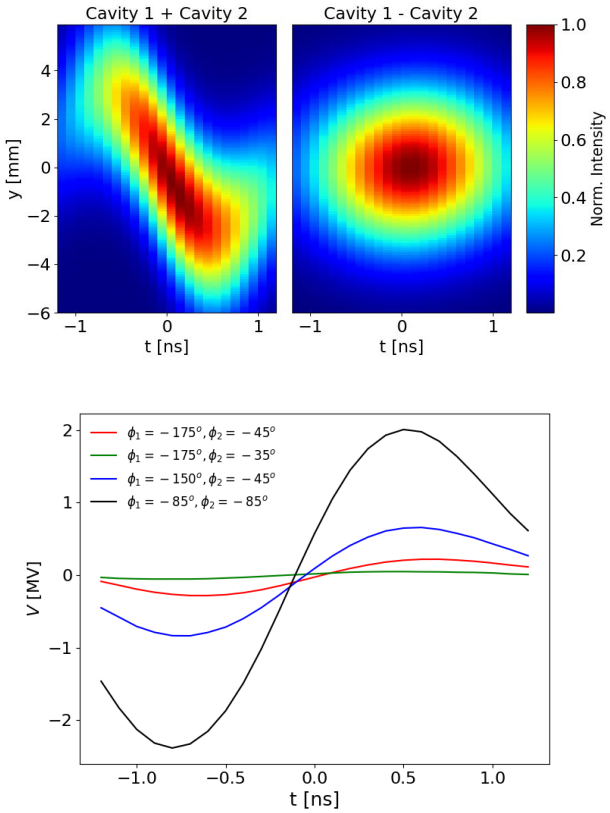

Fig. 7: Top: Simulation of cavities in an in-phase (left) and counter-phase modes (right) with 1 MV in each cavity. Bottom: HT monitor measurement; the green line corresponds to the phase where the transparency was achieved.

2 Update of the observation estimates for HL-LHC

2.1 Overview of available instrumentation

For the preparation of the SPS experiments the crabbed beam reading was simulated [6] and during the experiments the crab dispersion and the transparency of the cavities were observed with the Head-Tail (HT) monitor, the Wire Scanners (WS) and the Beam Position Monitors (BPMs) (see Sections 1.3 and 1.4). In a similar manner, during the HL-LHC CC commissioning, this type of instruments will be used to measure the crabbing for different beam and machine configurations at injection and collision energies for different β^* optics. In addition to the aforementioned instruments, the Beam Gas Vertex (BGV) and Synchrotron Radiation monitor, or beam transverse synchrotron light monitors (BSRT), could also be used to measure the crabbing of the beam.

In the presence of a CC kick the beam will have a crabbed Closed Orbit (CO) around the machine, i.e. different longitudinal slices within the bunch will have different closed orbits. For a given longitudinal slice, the CO will be deformed in a similar way as with a localised dipole error. The change in the CO due to a horizontal kick, as will be the case at IP1 where the crossing and CCs will be horizontal,

is given by Equation (1). The same equation holds in the case of a vertical kick at IP5 where we have vertical crossing and CCs; one only needs to use the vertical twiss functions and tune.

In the HL-LHC there will be a pair of CCs per beam, per Interaction Point (IP) side, i.e. 16 CCs in total, with a maximum achievable voltage of 3.4 MV each. For simulation purposes, each pair of CCs was treated as a single CC[1]; in MAD-X this was simulated with a static dipole kick of $\theta = V/E$, where V was set to the desired voltage and E was the beam energy (at injection E=450 GeV and at collision E=7000 GeV) using the HL-LHC v1.4 optics [7]. Each CC pair was switched ON one at a time, i.e. when the IP1-left pair was on, all others were OFF etc. Tables 2-5 list the twiss parameters at the location of each CC and each reading instrument at injection and collision energies for Beam1 and Beam2. Note that the CC-name indicates its location, e.g. ACFCA.AR1.B1 corresponds to the CC that is used for Beam1 (B1), at the right side of IP1 (R1); A and B indicate the proximity to the IP: A is closer to the IP than B is. The RMS bunch-length (FWHM equivalent Gaussian) at injection and collision energies is 9.2 cm and 9.0 cm respectively [8].

Table 2: Twiss parameters at the IP-, CC- and detector-location for Beam1, injection energy. The last two columns show the relative phase advance from IP1 (top) and IP5 (bottom); BSRT: MU.A5R4.B1, WS: BWS.5R4.B1, HT-H: BPLH.7R4.B1, HT-V: BPLV.A6R4.B1, HT A/B: the optional HT monitors

Name	**s [m]**	β_x **[m]**	β_y **[m]**	μ_x **[2π]**	μ_y **[2π]**	$d\mu_x$ **[π/2]**	$d\mu_y$ **[π/2]**
IP1	0.0	6.02	6.0	0.0	0.0	0.0	0.0
						0.1	0.17
IP5	13329.29	6.02	6.0	30.98	29.96	0.9	0.83
						0.0	0.0
ACFCA.AR1.B1	154.82	82.91	279.53	0.32	0.29	0.29	0.17
						0.38	0.34
ACFCA.BR1.B1	155.87	80.55	280.52	0.32	0.29	0.3	0.17
						0.39	0.34
ACFCA.BL5.B1	13169.6	283.77	72.55	30.68	29.62	0.72	0.5
						0.82	0.67
ACFCA.AL5.B1	13170.65	282.74	74.7	30.68	29.63	0.73	0.51
						0.82	0.68
ACFCA.AR5.B1	13484.11	82.77	279.43	31.3	30.25	0.19	0.99
						0.29	0.17
ACFCA.BR5.B1	13485.16	80.4	280.43	31.3	30.25	0.2	0.99
						0.29	0.17
ACFCA.BL1.B1	26499.2	283.21	72.57	61.98	59.96	0.9	0.85
						0.0	0.03
ACFCA.AL1.B1	26500.25	282.18	74.72	61.98	59.97	0.91	0.86
						0.0	0.04
MU.A5R4.B1	10042.71	206.43	351.16	23.46	22.25	0.85	0.01
						0.94	0.18
BWS.5R4.B1	10081.88	197.61	402.23	23.49	22.27	0.97	0.07
						0.07	0.25
BPLV.A6R4.B1	10134.76	253.08	401.18	23.53	22.29	0.14	0.15
						0.23	0.32
BPLH.7R4.B1	10174.96	544.96	51.52	23.55	22.34	0.2	0.36
						0.29	0.53
HT B.B1	9832.62	184.13	569.0	23.34	22.14	0.37	0.56
						0.47	0.73
HT A.B1	9859.75	397.67	302.68	23.36	22.15	0.44	0.6
						0.54	0.77

[1]The location of the cavity closer to the IP was chosen as the s-location of this pair.

Table 3: Twiss parameters at the IP-, CC- and detector-location for Beam1, collision energy. The last two columns show the relative phase advance from IP1 (top) and IP5 (bottom); BSRT: MBRS.5R4.B1, WS: BWS.5R4.B1, HT-H: BPLH.7R4.B1, HT-V: BPLV.A6R4.B1, HT A/B: the optional HT monitors

Name	**s [m]**	β_x **[m]**	β_y **[m]**	μ_x **[2π]**	μ_y **[2π]**	$d\mu_x$ **[π/2]**	$d\mu_y$ **[π/2]**
IP1	0.0	0.15	0.15	0.0	0.0	0.0	0.0
						0.28	0.04
IP5	13329.29	0.15	0.15	30.93	29.99	0.72	0.96
						0.0	0.0
ACFCA.AR1.B1	154.82	4256.24	3821.01	0.25	0.25	0.01	0.01
						0.28	0.05
ACFCA.BR1.B1	155.87	4133.64	3779.74	0.25	0.25	0.01	0.01
						0.28	0.05
ACFCA.BL5.B1	13169.6	3631.61	3702.45	30.68	29.74	0.71	0.95
						0.99	0.99
ACFCA.AL5.B1	13170.65	3672.05	3818.54	30.68	29.74	0.71	0.95
						0.99	0.99
ACFCA.AR5.B1	13484.11	4256.24	3821.03	31.18	30.24	0.73	0.96
						0.01	0.01
ACFCA.BR5.B1	13485.16	4133.64	3779.76	31.18	30.24	0.73	0.96
						0.01	0.01
ACFCA.BL1.B1	26499.2	3631.6	3702.43	62.06	60.07	0.23	0.27
						0.51	0.32
ACFCA.AL1.B1	26500.25	3672.05	3818.52	62.06	60.07	0.23	0.27
						0.51	0.32
MBRS.5R4.B1	10053.51	201.97	363.9	23.55	22.41	0.19	0.64
						0.47	0.69
BWS.5R4.B1	10081.88	197.01	402.01	23.57	22.42	0.29	0.69
						0.56	0.73
BPLV.A6R4.B1	10134.76	243.71	416.95	23.61	22.44	0.45	0.77
						0.73	0.81
BPLH.7R4.B1	10174.96	481.96	114.03	23.63	22.47	0.52	0.9
						0.8	0.94
HT B.B1	9832.62	181.35	573.77	23.42	22.29	0.69	0.17
						0.97	0.22
HT A.B1	9859.75	397.9	303.19	23.44	22.3	0.75	0.21
						0.03	0.26

Table 4: Twiss parameters at the IP-, CC- and detector-location for Beam2, injection energy. The last two columns show the relative phase advance from IP1 (top) and IP5 (bottom); BGV: BGVCA.B7L4.B2, WS: BWS.5L4.B2, BSRT: MU.A5L4.B2, HT-H: BPLH.6R4.B2, HT-V: BPLV.7R4.B2, HT A/B: the optional HT monitors

Name	**s [m]**	β_x **[m]**	β_y **[m]**	μ_x **[2π]**	μ_y **[2π]**	$d\mu_x$ **[π/2]**	$d\mu_y$ **[π/2]**
IP1	0.0	6.0	6.0	0.0	0.0	0.0	0.0
						0.91	0.09
IP5	13329.59	6.0	5.99	31.02	29.98	0.09	0.91
						0.0	0.0
ACFCA.AR1.B2	158.64	283.24	74.7	0.29	0.33	0.17	0.32
						0.09	0.41
ACFCA.BR1.B2	159.69	284.27	72.55	0.29	0.33	0.18	0.33
						0.09	0.42
ACFCA.BL5.B2	13173.73	80.81	280.3	30.7	29.69	0.79	0.74
						0.7	0.83
ACFCA.AL5.B2	13174.78	83.19	279.31	30.7	29.69	0.8	0.74
						0.71	0.84
ACFCA.AR5.B2	13488.23	282.84	74.86	31.31	30.31	0.26	0.23
						0.17	0.32
ACFCA.BR5.B2	13489.28	283.86	72.7	31.32	30.31	0.26	0.24
						0.18	0.33
ACFCA.BL1.B2	26503.02	80.58	280.31	61.95	60.0	0.79	0.01
						0.7	0.1
ACFCA.AL1.B2	26504.07	82.95	279.32	61.95	60.0	0.79	0.01
						0.71	0.11
BGVCA.B7L4.B2	9776.11	142.28	162.57	23.2	22.44	0.81	0.77
						0.72	0.86
BWS.5L4.B2	9912.28	196.94	451.74	23.29	22.53	0.15	0.11
						0.07	0.2
MU.A5L4.B2	9951.6	205.88	383.3	23.32	22.54	0.28	0.17
						0.19	0.26
BPLH.6R4.B2	10134.11	395.72	269.45	23.42	22.64	0.68	0.58
						0.6	0.67
BPLV.7R4.B2	10175.91	123.44	483.03	23.46	22.66	0.82	0.64
						0.74	0.74
HT B.B2	9832.77	469.41	208.73	23.23	22.5	0.93	0.99
						0.85	0.08
HT A.B2	9859.90	239.3	490.0	23.25	22.51	0.99	0.04
						0.9	0.13

Table 5: Twiss parameters at the IP-, CC- and detector-location for Beam2, collision energy. The last two columns show the relative phase advance from IP1 (top) and IP5 (bottom); BGV: BGVCA.B7L4.B2, WS: BWS.5L4.B2, BSRT: MBRS.5L4.B2, HT-H: BPLH.6R4.B2, HT-V: BPLV.7R4.B2, HT A/B: the optional HT monitors

Name	**s [m]**	β_x **[m]**	β_y **[m]**	μ_x **[2π]**	μ_y **[2π]**	$d\mu_x$ **[π/2]**	$d\mu_y$ **[π/2]**
IP1	0.0	0.15	0.15	0.0	0.0	0.0	0.0
						0.86	0.2
IP5	13329.59	0.15	0.15	31.03	29.95	0.14	0.8
						0.0	0.0
ACFCA.AR1.B2	158.64	3672.55	3818.29	0.25	0.25	0.01	0.01
						0.87	0.21
ACFCA.BR1.B2	159.69	3632.1	3702.21	0.25	0.25	0.01	0.01
						0.87	0.21
ACFCA.BL5.B2	13173.73	4134.1	3779.62	30.78	29.7	0.13	0.79
						0.99	0.99
ACFCA.AL5.B2	13174.78	4256.72	3820.89	30.78	29.7	0.13	0.79
						0.99	0.99
ACFCA.AR5.B2	13488.23	3672.45	3818.38	31.29	30.2	0.15	0.81
						0.01	0.01
ACFCA.BR5.B2	13489.28	3631.99	3702.29	31.29	30.2	0.15	0.81
						0.01	0.01
ACFCA.BL1.B2	26503.02	4134.21	3779.53	62.06	60.07	0.23	0.27
						0.1	0.47
ACFCA.AL1.B2	26504.07	4256.84	3820.79	62.06	60.07	0.23	0.27
						0.1	0.47
BGVCA.B7L4.B2	9776.11	143.18	168.84	23.15	22.51	0.6	0.05
						0.46	0.25
BWS.5L4.B2	9912.28	196.95	452.53	23.24	22.6	0.95	0.38
						0.81	0.59
MBRS.5L4.B2	9950.1	205.38	386.38	23.27	22.61	0.07	0.44
						0.93	0.64
BPLH.6R4.B2	10134.11	383.65	277.71	23.37	22.71	0.48	0.86
						0.34	0.06
BPLV.7R4.B2	10175.91	56.95	556.46	23.42	22.73	0.69	0.91
						0.56	0.12
HT B.B2	9832.77	466.54	211.57	23.18	22.57	0.73	0.26
						0.59	0.47
HT A.B2	9859.90	238.86	491.36	23.19	22.58	0.78	0.32
						0.64	0.52

Table 6: Instrumental resolution, independent of bunch intensity. In first approximation the HT resolution does not depend on intensity, as long as all bunches are of similar intensity and appropriate setup is performed for the circulating intensity [9–13]. The values in (*) were not available at the time this report was written; they are being calculated by the BI team.

Instrument	**Resolution**	**Accuracy**
HT [9]	0.1 mm	(*)
WS [10]	$<$10 μm, at least 3 pts/σ	5-10% (beam-size), at least 3 pts/σ
BSRT [11]	min. 10 μm beam-size change	(*)
BGV [12]	5% within 1 minute (bunch-by-bunch)	2% in 1 minute (average beam-size)
BPM [13]	100 μm (turn-by-turn) 1 μm (average orbit)	50 μm

2.2 Expected instrumentation performance at injection and collision energies

During the CC commissioning setup, 1-12 pilot bunches will be used. The crabbing for different bunch intensities will be read using BPMs and the HT monitor. Since during the 2018 SPS experiments the intensity was quickly increased from $2{\cdot}10^{10}$ ppb to the nominal one, it is expected that the nominal intensity will be used if the BPMs are shown to respond better at those values. The following procedure is expected to be followed:

1. Pilot beams with nominal intensity will be used at injection energy while the CCs are OFF. The injection oscillations, damper setting, and the overall orbit will be studied. The same topics can be studied with the CCs ON. During the 2018 SPS experiments it was shown that when the CCs were OFF the beam circulated without any issues. Additionally, the interlock will be checked for CC and main RF synchronisation, cavity trip, excess phase-change, etc.
2. The closed orbit will be scanned using the interaction region (IR) BPMs to bring the circulating beam as close as possible to the assumed mechanical centre.
3. The crabbing of the bunch induced from each CC pair starting from 1 MV will be measured using the HT monitors. The 1 MV is a safe value with respect to the machine protection and at the same time it gives a decent signal at injection (a different voltage may be used at collision energy).
4. Using the BPMs and the HT monitor a phase-scan routine will be performed to determine the crabbing-slope and deflection. In the SPS the HT cycle-by-cycle reading was used. The CC frequency will follow the main RF so in principle the synchronisation should be still present. An interlock is foreseen to dump the beam when the CCs and main RF are no longer synchronised (this interlock may be masked during commissioning).
5. The WS, BSRT and BGV monitors will be used as a complementary information to show the change of the bream-size due to crabbing.
6. In order to find the electrical centres at the injection ramp, we need at least 1-batch; 4-batches would be preferable to make a $\pm$ 5 mm orbit offset in steps of 0.5 mm and record induced voltage per two-cavity module. The way to do this is still to be devised as the orbit in the other cavities will be perturbed, unless the optics can create a closed bump in the crab region.
7. At injection energies, the voltage will be ramped in both crabbing and deflecting phase per two-cavity module to the nominal 3.4 MV. The beam loading, transparency, etc will be checked
8. In order to check what mode is more practical for operations, the energy ramp will be checked using pilot beams with the CCs OFF (the nominal operational scenario is with the CCs ON with $\sim$1 MV in anti-phase or smaller).
9. Most of the above steps will be repeated with collision optics (2 nominal beams should be enough). The electrical centre can be projected from the injection measurements.
10. The collision optimisation will be studied, including how to do vernier scans with CCs.

The following simulations were performed in order to study the instrumental performance at injection and collision energies. Since the BPM and HT reading has a linear relation with the CC-voltage, for these two instruments each pair of CCs was set to 1 MV; one can then easily scale the result according to the actual CC-voltage. This is not the case for the WS, BSRT and BGV monitors and therefore the CC-pair was set to the maximum achievable CC-voltage of 2·3.4 MV=6.8 MV. A quantitative description of what is expected to be measured by each instrument follows.

2.2.1 BPM

As with the SPS BPMs (see Section 1.3) a frequency filtering is applied to the LHC BPMs as well. The LHC BPM behaviour is modelled following the same procedure as in the case of the SPS MOPOS BPM, with the only difference being that this time the response $R(\omega)$ that appears in Eq. (4) has to be specialised to represent the LHC BPM transfer function. Note that, as shown in this equation, the BPM response strongly depends on the longitudinal distribution. The LHC BPMs have bunch-by-bunch capabilities, therefore a wide bandwidth filter is adopted in the front-end. The combined transfer function $R(\omega)$ of the LHC BPM pickup and front-end filter have been measured and are shown in Fig. 8. Taking

into account the 1 μm BPM resolution for the average orbit (see Table 6), Figure 9 shows the minimum voltage in V that can detect a 1 μm orbit for different CC-phases and a different applied BPM filter when the kick is applied at the ACFCA.AL5.B1 location. Table 7 shows the minimum detectable voltage for injection and collision optics for a CC-phase of 90 degrees. Note that these low voltage values may occur for example by an imperfect cancellation of the two CCs when operating with opposite phases. For the calculation of the minimum detectable voltage, Eq. (1) was also used, where $\beta(s)$ was replaced with the RMS β-value of all BPMs. In a similar manner, the minimum detectable voltage within the 50 μm BPM accuracy [13] is shown in Table 8 or injection and collision optics for a CC-phase of 90 degrees.

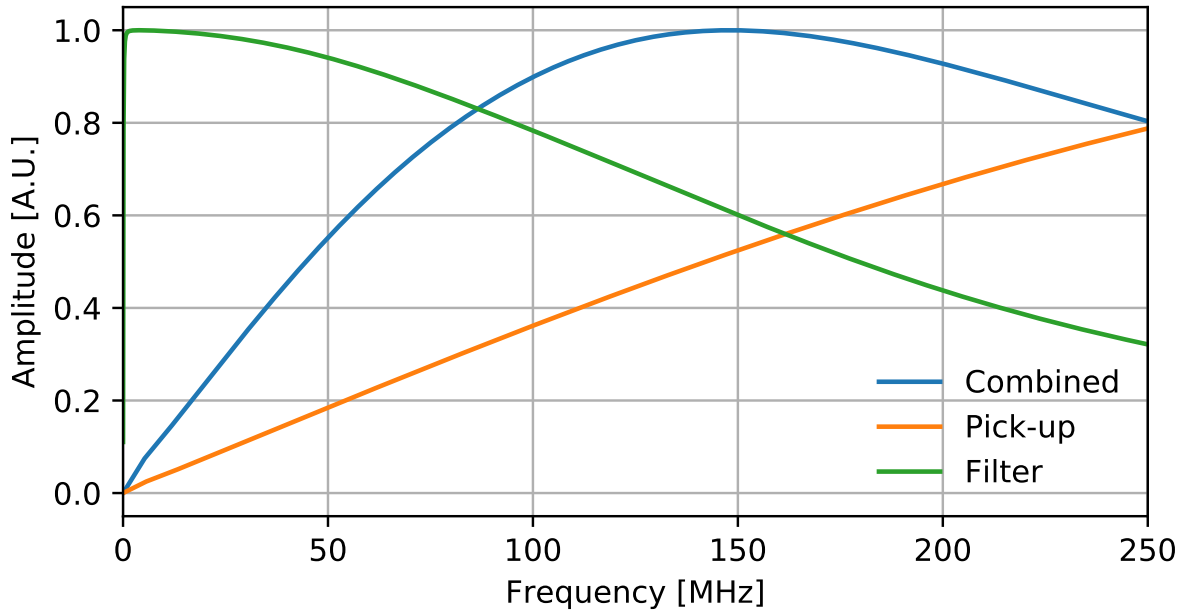

Fig. 8: Transfer functions for the LHC BPM pick-up, front-end and the combination of the two. To allow for bunch-by-bunch operation the front-end electronics is provided with a wide band low-pass filter with cut-off frequency of ~70 MHz.

Figure 10 shows a CO example at the BPM locations at injection and collision energies, when a 1 MV kick was applied at the ACFCA.AL5.B1 location (equivalent to the particles arriving at the crest of the CC-wave) while the other CCs were OFF. The CO was calculated with the analytical expression of Equation (1) (blue) as well as by MAD-X (cyan) without and with (red) a BPM filtering of 0.790 and 0.797 and for 90 degrees CC-phase at injection and collision energies respectively; a very good agreement is observed between the analytical and MAD-X calculation. The location of the CC-pair that was ON/OFF is indicated with red/pink vertical lines whereas the locations of the instruments are indicated with a blue vertical line. Note that the sensitivity of the measurement can be improved by fitting the induced CO distortion around the machine.

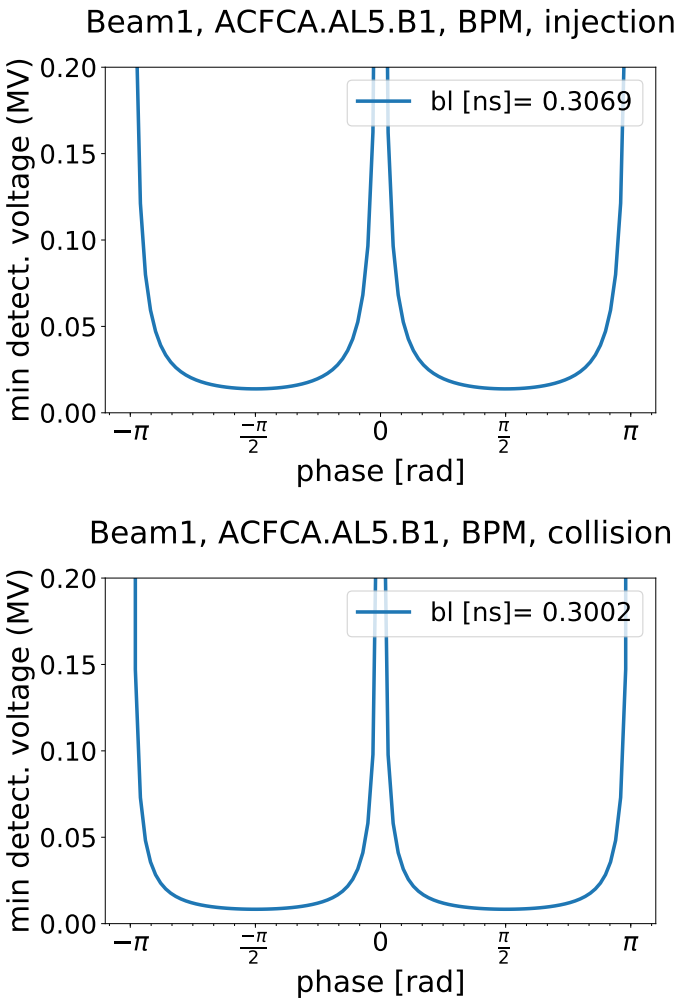

Fig. 9: BPM minimum detectable voltage within the 1 μm BPM resolution at injection (top) and collision (bottom) energies (bunch-length of 9.2 cm and 9.0 cm respectively assuming FWHM equivalent Gaussian), when ACFCA.AL5.B1 was set to 1 MV

Table 7: Minimum detectable voltage [MV] within the 1 μm BPM resolution for a CC-phase of 90 degrees

Injection	**L1**	**R1**	**L5**	**R5**
B1:	0.0061	0.0113	0.0138	0.0072
B2:	0.0114	0.0061	0.0071	0.0138
Collision	**L1**	**R1**	**L5**	**R5**
B1:	0.0079	0.0074	0.0083	0.0083
B2:	0.0074	0.0079	0.0083	0.0083

Table 8: Minimum detectable voltage [MV] within the 50 μm BPM accuracy for a CC-phase of 90 degrees

Injection	**L1**	**R1**	**L5**	**R5**
B1:	0.31	0.57	0.69	0.36
B2:	0.57	0.31	0.36	0.69
Collision	**L1**	**R1**	**L5**	**R5**
B1:	0.40	0.37	0.42	0.42
B2:	0.37	0.40	0.42	0.42

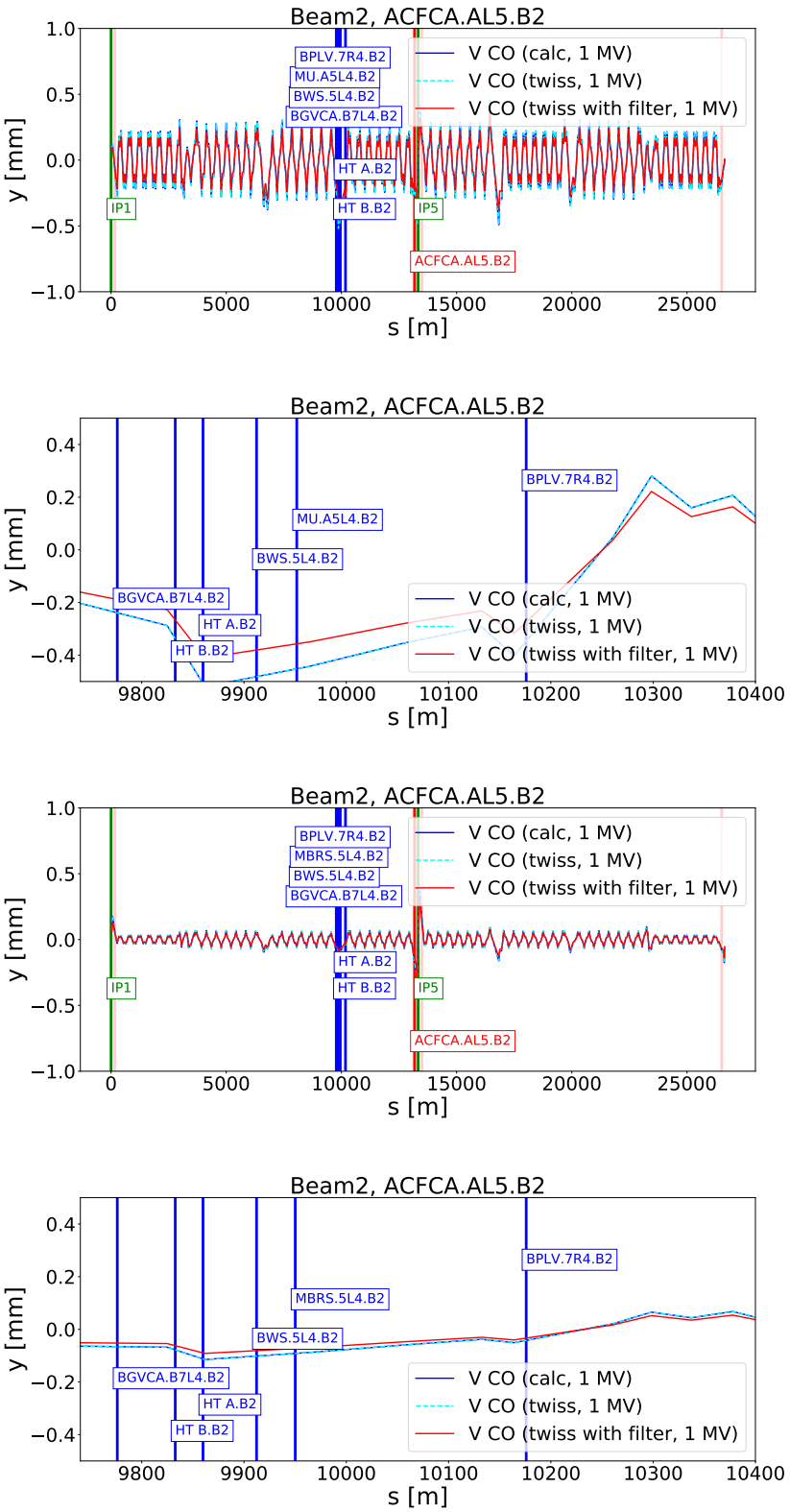

Fig. 10: BPM CO, B2, injection (top two) and collision (bottom two) energies when ACFCA.AL5.B2 was set to 1 MV

2.2.2 HT monitor reading

The Head-Tail (HT) monitor was designed to measure chromaticity and observe transverse instabilities, i.e. relatively large intra-bunch beam oscillations. It is therefore important to ensure that the transverse offset along the bunch due to the crabbing of the beam can be detected with the instrument's resolution

(see Table 6). In B1 the HT monitors are BPLH.7R4.B1 and BPLV.A6R4.B1, whereas BPLH.6R4.B2 and BPLV.7R4.B2 are installed for B2. There is also additional space reserved for optional HT monitors, for both beams and both planes, beside Q5L4 and Q6L4 in the positions of the existing BQKH.B6L4.B1 and BQKV.6L4.B1. These optional monitors are indicated as HT A/B in Tables 2-5 and Tables 9-10. The expected HT-reading for Beam1 at injection and collision energies, when ACFCA.AL5.B1 was set to 1 MV is presented in Figure 11. Table 9 summarises the maximum HT reading when 1 CC pair is ON at 1 MV at injection and collision energies for both beams.

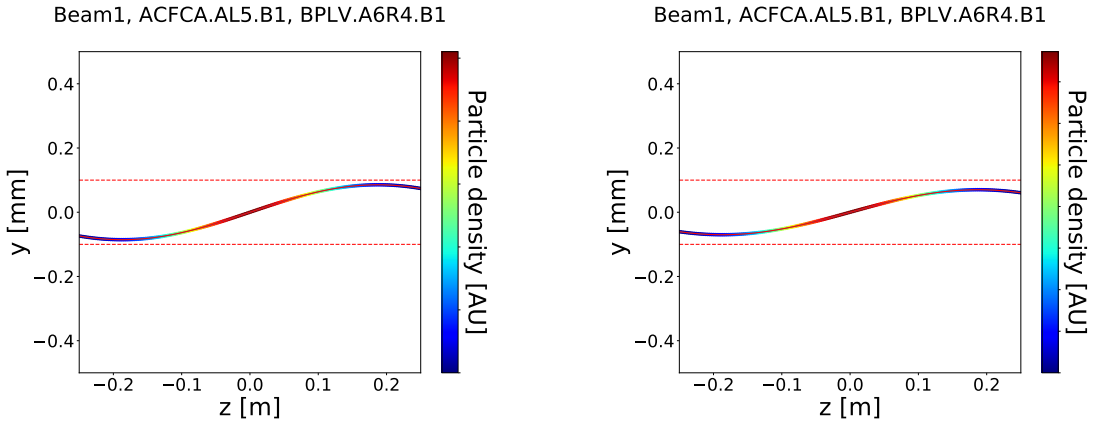

Fig. 11: HT readings for Beam1 at injection (left) and collision (right) energies, when ACFCA.AL5.B1 was set to 1 MV; dashed red lines: 0.1 mm resolution range.

Table 9: Maximum orbit at HT [mm] for a 1 MV kick; HT resolution: 0.1 mm

Injection	**L1**	**R1**	**L5**	**R5**
HT - B1	0.15	0.26	0.09	0.18
HT B.B1	0.34	0.14	0.15	0.54
HT A.B1	0.49	0.22	0.1	0.38
HT - B2	0.21	0.50	0.37	0.26
HT B.B2	0.26	0.18	0.32	0.09
HT A.B2	0.19	0.16	0.51	0.16
Collision	**L1**	**R1**	**L5**	**R5**
HT - B1	0.02	0.02	0.07	0.07
HT B.B1	0.07	0.08	0.03	0.03
HT A.B1	0.1	0.11	0.01	0.02
HT - B2	0.11	0.10	0.04	0.05
HT B.B2	0.02	0.02	0.07	0.08
HT A.B2	0.02	0.02	0.11	0.11

The expected orbit during operation (closed crab cavity bump) is given in Table 10 for two values of β^* representative of the beginning of the squeeze ($\beta^* = 50$ cm) and the end of the squeeze ($\beta^* = 15$ cm). It can be clearly seen this orbit is one or two orders of magnitude smaller than the HT resolution of 100 μm.

Table 10: Expected transverse orbit of particles at $z = \pm\sigma_z$ at the HT during operating conditions (closed crab cavity bump); the s-location is from IP1.

β^* = 50 cm	Position [m]	β_x [m]	β_y [m]	x [μm]	y [μm]
HT B - B1	9832.62	184.6	569.1	5.3	10.7
HT A - B1	9859.75	398.5	302.7	9.6	8.7
BPLV.A6R4.B1	10134.76	252.1	401.0	15.6	18.6
BPLH.7R4.B1	10174.96	543.0	51.5	22.8	6.6
HT B - B2	9832.77	467.4	210.2	21.2	2.5
HT A - B2	9859.90	238.0	492.7	15.2	5.6
BPLH.6R4.B2	10134.11	396.3	269.7	8.4	13.9
BPLV.7R4.B2	10175.91	123.6	483.3	2.5	19.4
β^* = 15 cm	Position [m]	β_x [m]	β_y [m]	x [μm]	y [μm]
HT B - B1	9832.62	181.3	573.8	2.8	11.0
HT A - B1	9859.75	397.9	303.2	5.2	8.3
BPLV.A6R4.B1	10134.76	243.7	416.9	8.3	9.1
BPLH.7R4.B1	10174.96	482.0	114.0	11.6	4.1
HT B - B2	9832.77	465.0	212.8	11.4	2.7
HT A - B2	9859.90	237.8	493.3	8.2	4.9
BPLH.6R4.B2	10134.11	383.7	277.7	5.2	8.1
BPLV.7R4.B2	10175.91	56.9	556.5	0.7	11.8

2.2.3 WS, BSRT, and BGV monitors

The possibility to measure the effect of crabbing on the beam-profile using the WS, the BSRT and the BGV monitors was investigated using a Gaussian distribution in both transverse and longitudinal planes. Note that for the BSRT optics functions, one has to look at the BSRT light source: at injection this is at the undulators MU.(A,B,C,D).5R4 for B1 and MU.(A,B,C,D).5L4 for B2, whereas at collision energy this is at the bending dipoles D3, MBRS.5R4 for B1 and MBRS.5L4 for B2. The MU.(A,B,C,D).5R4.B1 and MU.(A,B,C,D).5L4.B2 are only 14 cm apart, and their $\beta_{x,y}$ differ only between 0.03% and 0.06%. At injection energy, the optics at the MU.A.5R4.B1 and MU.A.5R4.B2 undulators were chosen to be used for the purpose of this study. Regarding the BGV monitor, they are is none in B1, and only one installed in B2: BGVCA.B7L4.B2 [14].

As the maximum achievable voltage per CC is 3.4 MV, Fig. 12 shows examples of the beam-profile without (red) and with a 6.8 MV kick at the ACFCA.AL5.B1 location (blue), at the WS (top), BSRT(middle) and BGV (bottom). The emittance difference after a kick of 6.8 MV at the location of each of the CC-pairs is given in Table 11 in units of μm (initial emittance: $2.5\ \mu$m); it varies from 0.0213 μm to 5.28 μm at injection and from 0.0019 μm to 3.8399 μm at collision energy. Table 12 and Table 13 provide the beam-size change due to the 6.8 MV kick at injection and collision energies, and show whether this change is within the resolution of the instruments or not. In the following cases the beam-size change does not fall within the resolution of the instruments: at injection energy, BSRT-B1 for L5, BGV-B1 for L1, BGV-B2 for R1 and R5; at collision energy, BGV-B1 and BGV-B2 for L1 and R1.

Table 11: Emittance change [μm] after a 6.8 MV kick at each CC-pair ($\epsilon_{init} = 2.5$ μm)

Injection	**L1**	**R1**	**L5**	**R5**
WS - B1	1.833	1.505	0.065	1.114
WS - B2	1.546	2.313	5.252	0.532
BSRT - B1	3.012	1.588	0.021	1.592
BSRT - B2	1.590	3.563	5.283	0.649
BGV - B2	0.884	0.110	3.418	0.047
Collision	**L1**	**R1**	**L5**	**R5**
WS - B1	0.821	1.065	1.109	1.026
WS - B2	0.994	0.798	3.381	3.446
BSRT - B1	1.312	1.670	0.859	0.785
BSRT - B2	1.792	1.463	3.096	3.174
BGV - B2	0.002	0.006	3.840	3.803

Table 12: Checking whether beam-size change is within instrumental resolution at injection

	CC	σ_{init} **[μm]**	σ_{end} **[μm]**	σ_{dif} **[μm]**	σ_{dif} **- 10 μm**	
WS-B1	L1	1018.56	1341.01	322.44	312.44	
	R1	1012.96	1282.03	269.07	259.07	
	L5	1447.97	1466.64	18.67	8.67	
	R5	1447.83	1740.83	293.00	283.00	
WS-B2	L1	1013.45	1289.24	275.80	265.80	
	R1	1013.24	1405.82	392.59	382.59	
	L5	1534.39	2701.97	1167.58	1157.58	
	R5	1534.53	1689.95	155.42	145.42	
BSRT-B1	L1	1038.82	1542.48	503.66	493.66	
	R1	1035.75	1324.55	288.79	278.79	
	L5	1352.94	1358.68	5.74	-4.26	
	R5	1352.76	1730.65	377.88	367.88	
BSRT-B2	L1	1036.23	1325.36	289.13	279.13	
	R1	1037.46	1615.59	578.13	568.13	
	L5	1413.34	2493.71	1080.36	1070.36	
	R5	1413.52	1586.53	173.00	163.00	
	CC	σ_{init} **[μm]**	σ_{end} **[μm]**	σ_{dif} **[μm]**	**0.05*σ_{init}**	σ_{dif} **[μm]-0.05*σ_{init}**
BGV-B1	L1	1324.93	1383.95	59.02	66.25	-7.23
	R1	1314.51	1555.47	240.96	65.73	175.23
	L5	356.01	431.72	75.71	17.80	57.91
	R5	356.08	450.60	94.53	17.80	76.72
BGV-B2	L1	861.16	1001.99	140.83	43.06	97.77
	R1	858.34	877.01	18.67	42.92	-24.25
	L5	920.64	1416.50	495.86	46.03	449.83
	R5	920.53	929.17	8.64	46.03	-37.39

Table 13: Checking whether beam-size change is within instrumental resolution at collision

	CC	σ_{init} [μm]	σ_{end} [μm]	σ_{dif} [μm]	σ_{dif} - 10 μm	
WS-B1	L1	257.29	296.56	39.27	29.27	
	R1	256.61	306.42	49.82	39.82	
	L5	367.04	440.99	73.95	63.95	
	R5	367.04	435.93	68.89	58.89	
WS-B12	L1	256.88	303.70	46.83	36.83	
	R1	256.91	295.09	38.18	28.18	
	L5	389.39	597.26	207.86	197.86	
	R5	389.39	600.54	211.14	201.14	
BSRT-B1	L1	260.49	321.67	61.18	51.18	
	R1	259.82	335.48	75.66	65.66	
	L5	349.21	404.81	55.60	45.60	
	R5	349.21	400.31	51.10	41.10	
BSRT-B2	L1	262.17	343.52	81.35	71.35	
	R1	262.50	330.50	68.00	58.00	
	L5	359.81	538.35	178.54	168.54	
	R5	359.81	542.05	182.24	172.24	
	CC	σ_{init} [μm]	σ_{end} [μm]	σ_{dif} [μm]	**0.05*σ_{init}**	σ_{dif} [μm]-0.05*σ_{init}
BGV-B1	L1	337.17	338.93	1.76	16.86	-15.09
	R1	336.59	339.89	3.30	16.83	-13.53
	L5	170.50	257.66	87.16	8.52	78.64
	R5	170.49	255.94	85.45	8.52	76.92
BGV-B2	L1	219.32	219.41	0.08	10.97	-10.88
	R1	218.74	218.98	0.24	10.94	-10.69
	L5	237.86	378.78	140.92	11.89	129.03
	R5	237.86	377.69	139.83	11.89	127.94

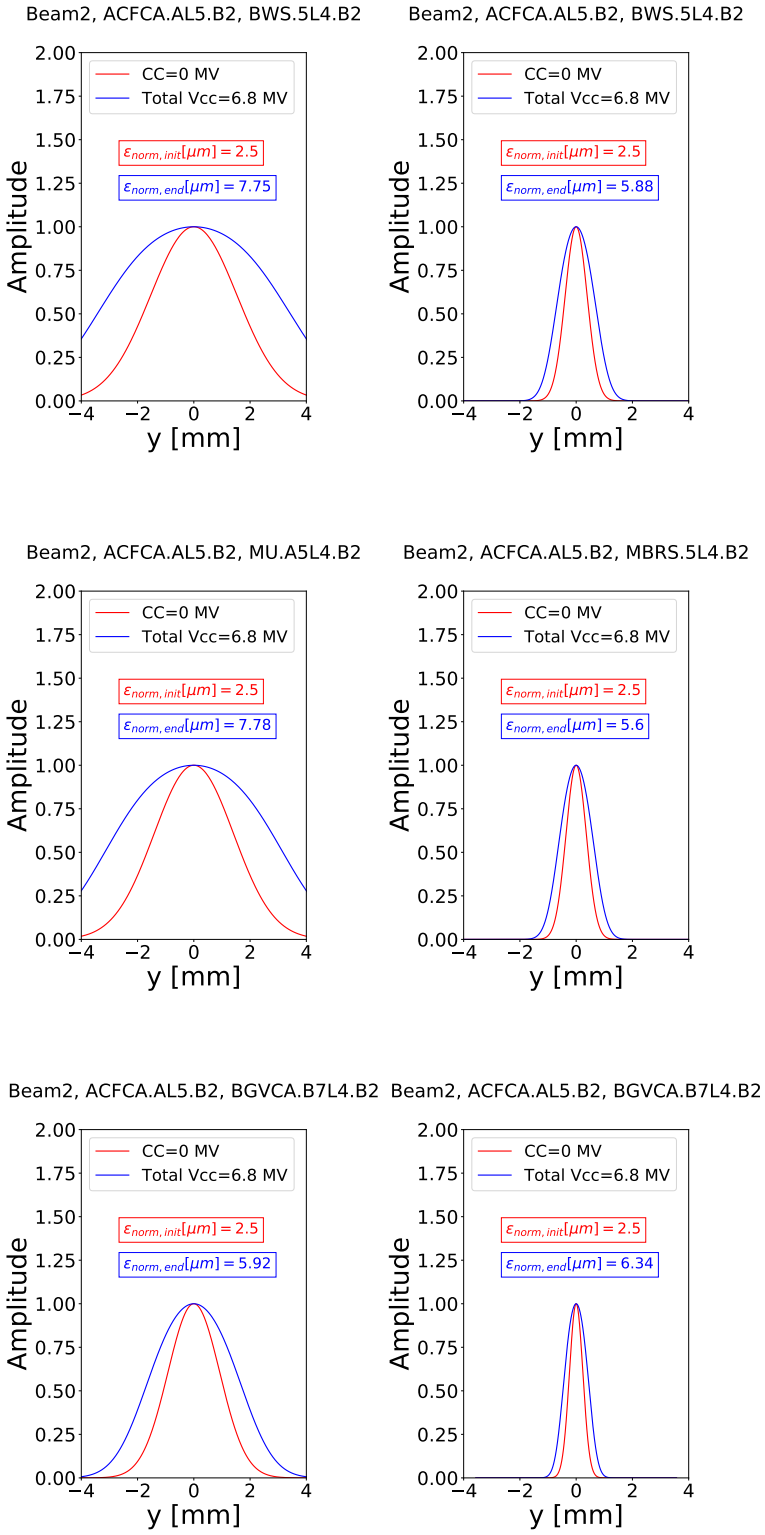

Fig. 12: WS (top), BSRT (middle) and BGV (bottom) projections for Beam2 at injection (left) and collision (right) energies, when ACFCA.AL5.B2 was set to 6.8 MV

2.3 Conclusions on the HL-LHC observation estimates

This note presents an overview of the available instrumentation and the observation estimates for HL-LHC at injection and collision energies. At HL-LHC there will be a total of 16 CCs: a pair per IP-side per beam. For this study, only 1 CC pair was ON each time. The following instruments are available to be

used during the CC-studies: BPMs that measure the charge centre with an applied filter, HT monitors to measure the transverse offset along the bunch due to the crabbing of the beam, and WS, BSRT and BGV monitors to measure the change in beam-profile. The minimum detectable voltage by BPMs (including the filtering) for a CC-phase of 90^{o} was found to be between 0.0061 MV and 0.0138 MV at injection energy and between 0.0074 MV and 0.0083 MV at collision energy. For a CC-voltage of 1 MV the HT reading is between 0.09-0.54 mm at injection and 0.01-0.11 mm at collision energy. The expected orbit during operation was calculated for two values of β^* representative of the beginning and end of the squeeze and it was found to be one or two orders of magnitude smaller than the HT resolution of 100 μm. Using the WS, BSRT and BGV monitor the emittance difference, from the initial emittance of 2.5 μm, when a voltage of 6.8 MV was applied was found to be between 0.0213 μm and 5.28 μm at injection and between 0.0019 μm and 3.8399 μm at collision energy. In the following cases the beam-size change due to this 6.8 MV kick does not fall within the resolution of the instruments: at injection energy, BSRT-B1 for L5, BGV-B1 for L1, BGV-B2 for R1 and R5; at collision energy, BGV-B1 and BGV-B2 for L1 and R1.

3 References

[1] L. Carver et al. First Machine Developments Result with HL-LHC Crab Cavities in the SPS. In *Proceedings, 10th International Particle Accelerator Conference (IPAC2019): Melbourne, Australia, May 19-24, 2019*, page MOPGW094, 2019.

[2] L. Carver. First proton beam dynamics results with crab cavities. Available at `https://indico.cern.ch/event/800428/attachments/1804664/2945632/CrabCavity_BE_Seminar.pdf`, 2019.

[3] P. Baudrenghien and T. Mastoridis. Transverse emittance growth due to rf noise in the high-luminosity LHC crab cavities. *Phys. Rev. Spec. Top. Accel. Beams*, 18(10):101001. 23 p, 2015.

[4] M. Carla' et al. Beam-based measurement of the skew-sextupolar component of the radio frequency field of a hl-lhc-type crab-cavity. MOPTS090, IPAC 2019.

[5] Y. Sun, R. Assmann, J. Barranco, R. Tomas, T. Weiler, F. Zimmermann, R. Calaga, and A. Morita. Beam dynamics aspects of crab cavities in the CERN Large Hadron Collider. *Phys. Rev. ST Accel. Beams*, 12:101002, 2009.

[6] A. Alekou, F. Antoniou, R. Appleby, G. Arduini, H. Bartosik, R. Calaga, Y. Papaphilippou, and C. Welsch. SPS Studies in Preparation for the Crab Cavity Experiment. In *Proceedings, 8th International Particle Accelerator Conference (IPAC 2017): Copenhagen, Denmark, May 14-19, 2017*, page TUPVA034, 2017.

[7] `https://ref.ipac19.org/reference/show/92310`.

[8] E. Metral et al. Update of the HL-LHC operational scenarios for proton operation. Jan 2018.

[9] Private communication with T. Levens.

[10] Private communication with F. Roncarolo.

[11] Private communication with G. Trad.

[12] Rhodri Jones. Current cern beam instrumentation group baseline for beam size measurements in the high luminosity lhc era. `https://indico.cern.ch/event/837340/contributions/3510891/attachments/1916883/3169408/Beam_Size_Measurement_review_-_WP13_baseline_2019.pdf`, 2-3 October 2019.

[13] Private communication with M. Krupa.

[14] Private communication with J. Storey.